NJC

ROYAL SOCIETY OF CHEMISTRY

PAPER

View Article Online
View Journal | View Issue



Cite this: *New J. Chem.*, 2024, **48**, 2416

# The effect of rigidity on the emission of quadrupolar strongly polarized dyes†

Bartosz Szymański,[ad] Smruti Ranjan Sahoo,[b] Rashid Valiev,[c] Olena Vakuliuk,[a] Piotr Łaski,[d] Katarzyna N. Jarzembska,[d] Radosław Kamiński,[d] Glib Baryshnikov,*[bf] Mohammad B. Teimouri*[ae] and Daniel T. Gryko*[a]

Received 28th November 2023,
Accepted 3rd January 2024

DOI: 10.1039/d3nj05467e

rsc.li/njc

Hybrid dyes comprising 1,4-dihydropyrrolo[3,2-*b*]pyrrole and two strongly electron-withdrawing benzoxadiazole substituents, differing in their level of planarization, offer an insightful window into the interplay between internal conversion and intersystem crossing as relaxation pathways from the excited state. The emission intensity is strong for non-fused systems whilst it is minimal for fused dyes. Computational evaluation has revealed that internal conversion, and not inter-system crossing, is the main non-radiative process for planar, fused quadrupolar dyes.



## Introduction

Centrosymmetric dyes with acceptor–donor–acceptor (A–D–A) and donor–acceptor–donor (D–A–D) architectures,[1–5] which form emissive CT states, can display solvatofluorochromism, caused by excited-state symmetry breaking (ES-SB).[6–10] Many new quadrupolar,[11–14] centrosymmetric systems have been reported over the last few years, but there has been no consensus on the influence of restricted rotation (rigidity) on the emission properties, ES-SB and thermodynamics of intramolecular charge transfer (ICT).[15]

In this regard we hypothesized that it could be possible to directly study the influence of restricted rotation on the fate of quadrupolar dye molecules in the excited state by bridging strongly electron-donating and electron-deficient moieties. Assessing this hypothesis requires two dyes possessing identical, quadrupolar scaffolds except for their degrees of rigidity. Designing the quadrupolar architectures, we considered several candidates for the electron-rich scaffold, but we eventually decided upon 1,4-dihydropyrrolo[3,2-*b*]pyrrole (DHPP) due to the combination of the following properties: (1) exceptionally high-lying HOMO; (2) straightforward and modular synthesis; (3) possibility of vast structural modification.[16–18] The combination of these features has been utilized several times, predominantly to decipher the fluorescence of nitro-aromatics.[19,20] Simultaneously, we reasoned that incorporation of 2,1,3-benzoxadiazole[21–24] at the strongly conjugated positions 2 and 5 of DHPP represents an optimal choice as an electron-acceptor. The versatility and generality of the multicomponent reaction affording tetraarylpyrrolo[3,2-*b*]pyrroles (TAPPs)[25] enabled us to assemble the required quadrupolar dye **1** in just one step (Scheme S1 (ESI†) and Fig. 1). Subsequently the benzo[*c*][1,2,5]oxadiazole-4-carbaldehyde (**2**) was condensed with 2-bromo-4-octadecylaniline (**3**) affording TAPP **5**, which was subjected to intramolecular direct arylation,[26] giving almost planar quadrupolar centrosymmetric architecture **6** (Scheme 1).

The photophysical properties of dyes **1** and **6** were studied in solvents of various polarity and in the polycrystalline state

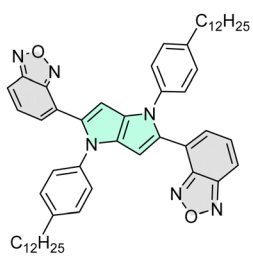


**1**

Fig. 1 Structural formula of centrosymmetric TAPP **1**.

[a] *Institute of Organic Chemistry, Polish Academy of Sciences, Kasprzaka 44/52, 01-224, Warsaw, Poland. E-mail: dtgryko@icho.edu.pl*
[b] *Laboratory of Organic Electronics, Department of Science and Technology, Linköping University, SE-60174, Norrköping, Sweden. E-mail: glib.baryshnikov@liu.se*
[c] *Department of Chemistry, University of Helsinki, FI-00014, Helsinki, Finland*
[d] *Department of Chemistry, University of Warsaw, Żwirki i Wigury 101, 02-089 Warsaw, Poland. E-mail: rkaminski85@uw.edu.pl*
[e] *Faculty of Chemistry, Kharazmi University, 15719-14911 Tehran, Iran. E-mail: teimouri@khu.ac.ir*
[f] *Department of Chemistry and Nanomaterials Science, Bohdan Khmelnytsky National University, 18031 Cherkasy, Ukraine*

† Electronic supplementary information (ESI) available: Synthesis, compound characterization, X-ray structural data, supporting spectroscopic plots, computational details, computed spectroscopic characteristics, Cartesian coordinates for optimized structures and spectral data for all new compounds. CCDC 2288872. For ESI and crystallographic data in CIF or other electronic format see DOI: https://doi.org/10.1039/d3nj05467e

 

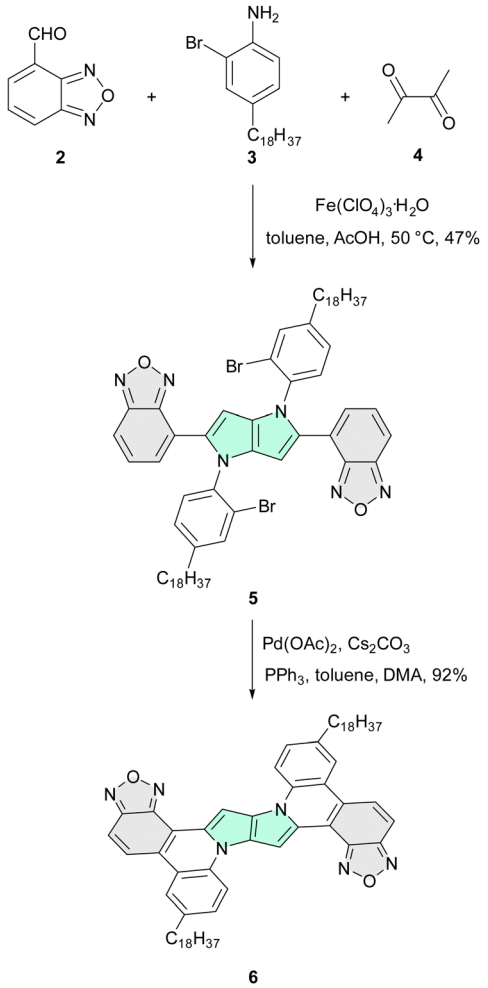


Scheme 1 Synthesis of dye **6**.

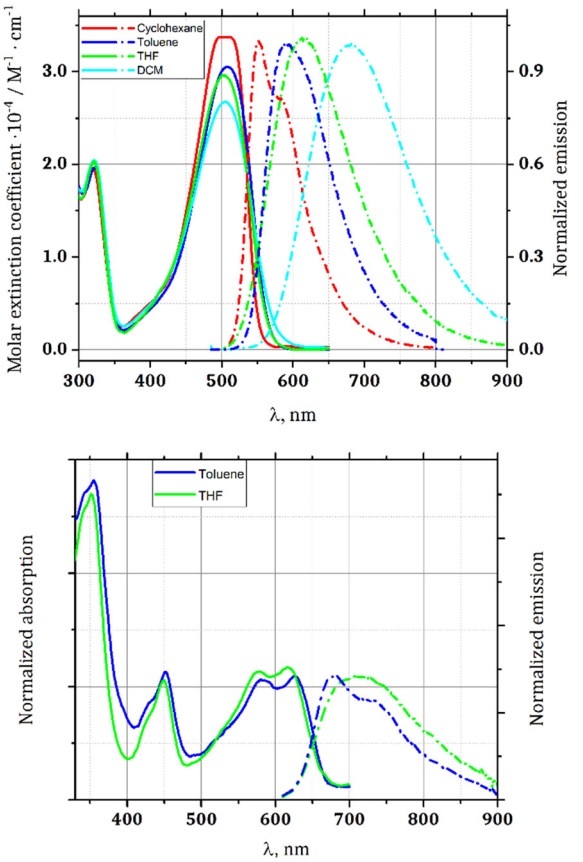


Fig. 2 Absorption (solid lines) and emission (dot-dashed lines) spectra of TAPP **1** (upper) and **6** (lower).

(Table 1 and Fig. 2). The presence of the strongly electron-withdrawing benzoxadiazole substituents shifts the absorption and emission about 1900–2300 $cm^{-1}$ bathochromically with respect to the analogous TAPP possessing two 4-nitrophenyl substituents at positions 2 and 5,[19] and makes TAPP **1** susceptible to changes in solvent polarity. Dye **1** exhibits strong fluorescence in non-polar solvents, characterized by a relatively low Stokes shift (Table 1). However, the fluorescence is quenched in polar solvents due to the presence of specific non-radiative relaxation pathways, namely charge-transfer-type transitions, and vibrational relaxation of the polar excited state. Solvents such as toluene, tetrahydrofuran (THF) or dichloromethane (DCM) effectively stabilize this state, resulting in larger Stokes shifts (Fig. 2).

Table 1 Photophysical data for dyes **1** and **6**

| Dye | Solvent or powder | $\lambda_{abs}^{max}$/nm ($\varepsilon$ $10^{-4}$/$M^{-1}$ $cm^{-1}$) | $\lambda_{em}^{max}$/nm | $\Phi_{f1}$ | $\Delta\tilde{\nu}$/$cm^{-1}$ |
|---|---|---|---|---|---|
| **1** | Cyclohexane | 499 (29) | 553 | 0.77[a] | 2000 |
| | Toluene | 506 (25) | 590 | 0.67[a] | 2800 |
| | THF | 501 (25) | 623 | 0.44[a] | 3900 |
| | DCM | 504 (23) | 673 | 0.08[a] | 5000 |
| | Cryst. powd. | 518 | 582 | 0.20[b] | 2100 |
| **6** | Toluene | 354, 452, 580, 626 | 683, 724 (sh) | 0.11[c] | 1330 |
| | THF | 351, 448, 576, 637 | 714 | 0.03[c] | 1700 |
| | Cryst. powd. | 678 | 743 | <0.01[b] | 1300 |

[a] Reference: rhodamine 6G in EtOH ($\Phi_{f1}$ = 0.95). [b] Measured with an integrating sphere. [c] Reference: oxazine **1** in MeOH ($\Phi_{f1}$ = 0.11).

On the other hand, rigid and planar (vide infra) dye **6** shows remarkably different characteristics. Predominantly, it has extremely low solubility in the majority of solvents. Careful experiments have proven that in many solvents, it does not form real solutions but rather an ultrafine suspension, which cannot pass through a 0.45 μm syringe filter. Consequently, its photophysical studies were conducted only in toluene and in THF. The large size and planarity of the chromophore inclined us to investigate the possibility to form aggregates. The measurements of the dependence of the absorption on the concentration, performed in toluene, have proven that there is no aggregation within the measured concentration range.

The emission maximum for compound **6** is bathochromically shifted to 683 nm in toluene. Noteworthily, **6** possesses a more rigid chromophore compared to **1** and thus in the excited state it is less exposed to the vibronic relaxation pathways. Hence, compound **6** deactivates with the geometry close to the 1FC* state with preserved vibronic structure in the emission spectra (in toluene), while for compound **1** the detailed

vibrational structure is lost and the emission spectrum appears as a broad band for most of the cases.

Compound **6** exhibits weak fluorescence, getting even lower in more polar THF, whereas solvatofluorochromism is weaker, but it remains observable (Table 1). It is worth noting that Stokes shifts are significantly lower for compound **6**. They also do not correlate with solvent polarity. For compound **1** they are, however, enormous in polar solvents, providing bathochromic shift of emission (Table 1). Here, planarization causes a strikingly different effect to when nitro groups play the role of electron-withdrawing substituents.[27]

TAPP **1** crystallizes in the triclinic $P\bar{1}$ space group with two halves of two symmetry-inequivalent molecules in the asymmetric unit (Fig. 3). The C4–C5–C7–N1 and C7–N1–C10–C11 torsion angles are 26.4(5)° and 33.0(4)°, respectively. The distance between C4 and C11 carbon atoms (which are bound in **6**) is 3.098(4) Å in the crystal structure of **1**. The main influence on the stability of the crystal structure stems from van der Waals interactions between the long alkyl chains, which results in a layered architecture of the crystal (Fig. 3). There is a hydrogen bond between two TAPP molecules namely C38–H38···N2 (Fig. S11, ESI†).

Having the single crystal structure in hand, we performed solid-state photophysical measurements. As far as the solid-state emission is concerned, both examined quadrupolar dyes, **1** and **6**, exhibit strikingly different properties. In the case of TAPP **1**, there are two emission maxima of a single crystal at room temperature, located around 460 nm and 580 nm, and the excited-state lifetime is estimated to be 3.800(9) ns (Fig. S7, ESI†). For dye **6**, owing to the fused benzene rings when compared to **1**, two emission maxima are notably red-shifted to about 550 nm and 745 nm. As expected, the emission decay of **6** is much faster than that of **1**. The respective room-temperature lifetime is estimated to be *ca.* 1 ns, which is at the accuracy limit of the spectroscopic setup used (Fig. S7, ESI†). It should also be noted that temperature has a greater effect on the emission decay of **6**. When lowering the temperature to 100 K, the emission maximum gets red-shifted ≈35 nm, to *ca.* 780 nm with almost no effect on emission lifetime. In the case of dye **1** no significant temperature-dependent spectral changes are observed.

Fluorescence quantum yields in the solid state are markedly different for both compounds. Whereas **1** exhibits a 20% quantum yield, which is considered moderate, dye **6** is almost not fluorescent at all. This corresponds well with results obtained from measurements in various solvents.

The TD DFT optimized excited states ($S_1$) of both **1** and **6** do not significantly differ from their corresponding ground state ($S_0$) geometries. Apparently, when going from the $S_0$ to the $S_1$ state, it is observed that the dihedral angles change in the range 0.2°–7.8° and 0.5°–4.5° between the benzoxiadiazolyl group and DHPP and the benzoalkyl group and DHPP, respectively for non-fused dye **1**; whereas these values are calculated to be nearly zero for fused dye **6**, *i.e.* 0.02°–0.13° and 0.02°–0.34°, supporting the rigidity and planarity of dye **6** in the excited state.

Computational calculations using the TD-DFT/PCM/B3LYP-37/6-31G(d,p) formalism were in good agreement with the experimental photophysical properties of dyes **1** and **6** (Table 1). The main absorption and emission bands correspond to the intramolecular HOMO → LUMO charge-transfer transition (Fig. 4).

The calculated $S_1 \rightarrow S_0$ radiative rates ($k_r$) of dye **1** in different solvents are approximately the same ($2.0 \times 108\ s^{-1}$),

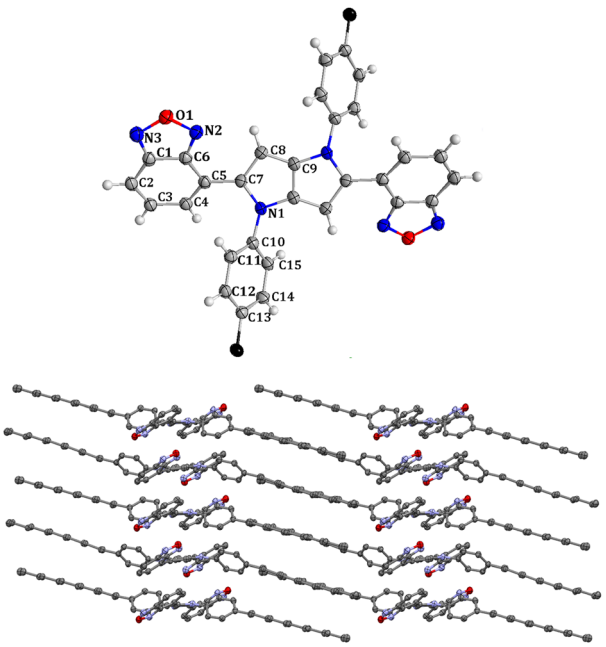


Fig. 3 Molecular structure of **1** (upper). Torsion angles and the distance between C4 and C11 in the **1** crystal structure. Note that ellipsoids correspond to 50% probability of atom location. Alkyl chains and hydrogen atoms are omitted for clarification. Packing in the crystal of **1** (lower). There are some intermolecular interactions between aryl rings, which probably stabilize the structure.

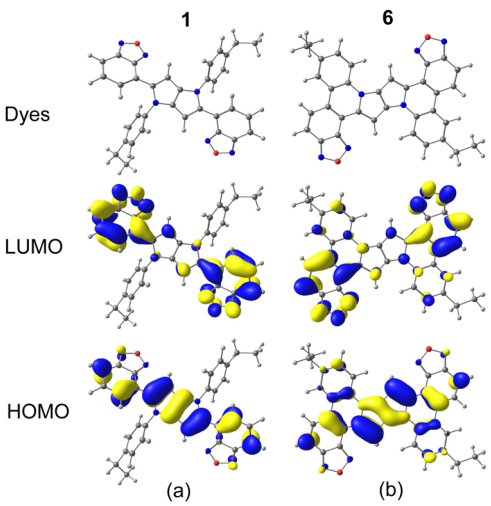


Fig. 4 Calculated optimized ground ($S_0$) state structures of dye **1** (a) and **6** (b) with ethyl chains and isosurfaces for the highest occupied molecular orbital (HOMO) and lowest unoccupied molecular orbital (LUMO). The calculated $E_{HOMO}/E_{LUMO}$ values for dye **1** (a) and **6** (b) are −5.55/−1.99 eV and −5.41/−2.21 eV, respectively. Both $S_0 \rightarrow S_1$ optical absorption and $S_1 \rightarrow S_0$ emission correspond to HOMO → LUMO electronic transition.

 

Table 2 Summary of perturbative spin–orbit coupling excitation calculations, intersystem crossing (ISC), internal conversion (IC) and radiative rate constants of **1** and **6**

| Dye | Solvent | $E_{S_1}$/eV | $E_{T_1}$/eV | $E_{T_2}$/eV | $SOCME_{S_1T_1}$/ $cm^{-1}$ | $SOCME_{S_1T_2}$/ $cm^{-1}$ | $k_{ISC}^{S_1T_1} \times 10^2 / s^{-1}$ | $k_r{}^a \times 10^8/s^{-1}$ | $k_{IC}{}^b \times 10^8/s^{-1}$ | $\phi_{fl}^{theor}(\phi_{fl}^{exp})$ |
|---|---|---|---|---|---|---|---|---|---|---|
| **1** | Cyclohexane | 1.99 | 1.11 | 1.62 | 0.04 | 0.37 | 2.06 | 2.053 | 1.0 | 0.61 (0.77) |
| | Toluene | 1.97 | 1.10 | 1.61 | 0.03 | 0.37 | 1.35 | 2.053 | 1.0 | 0.58 (0.67) |
| | THF | 1.83 | 1.05 | 1.57 | 0.03 | 0.39 | 12.8 | 2.027 | 2.3 | 0.32 (0.44) |
| | DCM | 1.81 | 1.05 | 1.56 | 0.03 | 0.39 | 13.7 | 2.023 | 2.4 | 0.31 (0.08) |
| **6** | Cyclohexane | 1.64 | 1.02 | 1.53 | 0.02 | 0.00 | 16.2 | 0.738 | 4.3 | 0.14 |
| | Toluene | 1.62 | 1.01 | 1.52 | 0.02 | 0.00 | 17.9 | 0.752 | 4.7 | 0.13 (0.11) |
| | THF | 1.53 | 0.98 | 1.48 | 0.01 | 0.00 | 27.8 | 0.805 | 7.0 | 0.10 (0.03) |
| | DCM | 1.52 | 0.98 | 1.48 | 0.01 | 0.00 | 29.1 | 0.810 | 7.5 | 0.09 ($<$ 0.01) |

while for fused dye **6** the radiative rate is approximately three times smaller (0.7–0.8 $\times$ 108 $s^{-1}$). We found two triplet states ($T_1$ and $T_2$) energetically lower than the $S_1$ state for both dyes. The spin–orbit coupling matrix elements (SOCMEs) between $S_1$ and $T_1$ states for both **1** and **6**, however, are negligibly small (less than 0.05 $cm^{-1}$) while the $S_1$–$T_1$ energy gap is considerable (0.7–0.9 eV for **1** and near 0.6 eV for **6**) which results in a calculated rate of $S_1 \rightarrow T_1$ intersystem crossing $\left(k_{ISC}^{S_1T_1}\right)$ of $10^2$–$10^3$ $s^{-1}$ order of magnitude (Table 2 and Table S8, ESI†), *i.e.* uncompetitive with the radiative rate. At the same time, the $S_1$–$T_2$ gap is much smaller for both **1** and **6**, while SOCME between the $S_1$ and $T_2$ states for **1** is large (near 0.4 $cm^{-1}$). This results in $k_{ISC}^{S_1T_2}$ for **1** being in region of 0.36–2.0 $\times$ $10^8$ $s^{-1}$, *i.e.* it is comparable with the radiative rate constant. However, for compound **6** the SOCME between the $S_1$ and $T_2$ states is predicted to be zero, which corresponds to a zero rate constant for $k_{ISC}^{S_1T_2}$. This means that fluorescence quenching for dye **6** originates from $S_1$–$S_0$ internal conversion (IC). Indeed, our calculations predict $k_{IC}$ for compound **6** to increase with an increase of solvent polarity from 4.3 $\times$ $10^8$ $s^{-1}$ in cyclohexane to 7.5 $\times$ $10^8$ $s^{-1}$ in DCM. For compound **1**, internal conversion also significantly contributes to fluorescence quenching and demonstrates a similar solvent polarity dependence as for fused dye **6**. The calculated values of fluorescence quantum yield ($\phi_{fl}^{theor}$) estimated as a relation between radiative rate and the sum of radiative and all non-radiative rate constants finally demonstrates a good agreement with the experimental measurements (Table 2 and Table S8, ESI†).

## Conclusions

In conclusion, by planarization of the geometry of highly polarized, centrosymmetric dyes, it is possible to gain control over the fate of the molecular excited state. Furthermore, our observations indicate that while balanced donor–acceptor coupling ensures fast radiative deactivation and slow ISC essential for large fluorescence quantum yields, planarization changes this balance towards IC. Planarization reduces spin–orbit coupling matrix elements between the singlet and triplet excited states to essentially zero, shifting the main mechanism of non-radiative deactivation from $S_1$ to $S_0$ from intersystem crossing to internal conversion. These mechanistic paradigms set important design principles for molecular photonics and electronics.

## Author contributions

Conceptualization: D. T. G. and M. B. T.; investigation: B. S., O. V., M. B. T., P. Ł., S. R. S., R. V.; supervision: D. T. G., G. B., R. K., K. N. J.; visualization: D. T. G., B. S., P. Ł.; writing – original draft: B. S., D. T. G., O. V., G. B., P. Ł., R. K., K. N. J.; writing – review and editing: D. T. G., O. V., R. K., K. N. J., G. B.

## Conflicts of interest

There are no conflicts to declare.

## Acknowledgements

This work was supported by the Polish National Science Center, Poland (grants OPUS 2020/37/B/ST4/00017 and 2019/33/B/ST4/03144), and by grant no. 324139 of the Research Council of Norway (AG). G. B. thank the Ministry of Education and Science of Ukraine for support (Project No. 0121U107533). We thank K. Durka (Warsaw, Poland) for his help with solid-state quantum-yield measurements. The X-ray diffraction experiments were carried out at the Department of Physics, University of Warsaw, on a Rigaku Oxford Diffraction SuperNova diffractometer, which was co-financed by the European Union within the European Regional Development Fund (program no. POIG.02.01.00-14.122/09). The quantum-chemical calculations were performed with computational resources provided by the National Academic Infrastructure for Supercomputing in Sweden (NAISS 2023/5-77) at the National Supercomputer Centre (NSC) at Linköping University partially funded by the Swedish Research Council through grant agreement no. 2022-06725. G. B. thanks the support by the Swedish Research Council through starting grant no. 2020-04600. G. B. and S. R. S. are also thankful for support from Olle Engkvists Stiftelse (Sweden), project number 212-0136.

## Notes and references

1 Y. Feng, P. J. Das, R. M. Young, P. J. Brown, J. E. Hornick, J. A. Weber, J. S. W. Seale, C. L. Stern, M. R. Wasielewski and J. F. Stoddart, *J. Am. Chem. Soc.*, 2022, **144**, 16841–16854.
2 R. Feng, N. Sato, T. Yasuda, H. Furuta and S. Shimizu, *Chem. Commun.*, 2020, **56**, 2975–2978.

3 S. Shimizu, A. Murayama, T. Haruyama, T. Iino, S. Mori, H. Furuta and N. Kobayashi, *Chem. – Eur. J.*, 2015, **21**, 12996–13003.
4 T. M. Cooper, J. E. Haley, D. M. Krein, A. R. Burke, J. E. Slagle, A. Mikhailov and A. Rebane, *J. Phys. Chem. A*, 2017, **121**, 5442–5449.
5 C. L. Anderson, T. Zhang, M. Qi, Z. Chen, C. Yang, S. J. Teat, N. S. Settineri, E. A. Dailing, A. Garzón-Ruiz, A. Navarro, Y. Lv and Y. Liu, *J. Am. Chem. Soc.*, 2023, **145**, 5474–5485.
6 Z. Szakács and E. Vauthey, *J. Phys. Chem. Lett.*, 2021, **12**, 4067–4071.
7 B. Dereka, A. Rosspeintner, Z. Li, R. Liska and E. Vauthey, *J. Am. Chem. Soc.*, 2016, **138**, 4643–4649.
8 F. Terenziani, A. Painelli, C. Katan, M. Charlot and M. Blanchard-Desce, *J. Am. Chem. Soc.*, 2006, **128**, 15742–15755.
9 T. Kim, J. Kim, H. Mori, S. Park, M. Lim, A. Osuka and D. Kim, *Phys. Chem. Chem. Phys.*, 2017, **19**, 13970–13977.
10 T. Beppu, K. Tomiguchi, A. Masuhara, Y.-J. Pu and H. Katagiri, *Angew. Chem., Int. Ed.*, 2015, **54**, 7332–7335.
11 (*a*) Y. Hong, F. Schlosser, W. Kim, F. Würthner and D. Kim, *J. Am. Chem. Soc.*, 2022, **144**, 15539–15548; (*b*) R. H. Kim, J. S. Park, K.-S. Lee, K. Zojer and J.-L. Brédas, *Int. J. Quantum Chem.*, 2017, e25441; (*c*) Z. Szakács, F. Glöcklhofer, F. Plasser and E. Vauthey, *Phys. Chem. Chem. Phys.*, 2021, **23**, 15150–15158; (*d*) J. A. Clark, D. Kusy, O. Vakuliuk, M. Krzeszewski, K. J. Kochanowski, B. Koszarna, O. O'Mari, D. Jacquemin, T. Gryko and V. I. Vullev, *Chem. Sci.*, 2023, **14**, 13537–13550.
12 E. Vauthey, *J. Phys. Chem. Lett.*, 2022, **13**, 2064–2071.
13 M. Söderberg, B. Dereka, A. Marrocchi, B. Carlotti and E. Vauthey, *J. Phys. Chem. Lett.*, 2019, **10**, 2944–2948.
14 C. W. Stark, M. Rammo, A. Trummal, M. Uudsemaa, J. Pahapill, M.-M. Sildoja, S. Tshepelevitsh, I. Leito, D. C. Young, B. Szymański, O. Vakuliuk, D. T. Gryko and A. Rebane, *Angew. Chem., Int. Ed.*, 2022, **61**, e202212581.
15 N. I. Nijegorodov and W. S. Downey, *J. Phys. Chem.*, 1994, **98**, 5639–5643.
16 M. Krzeszewski, D. Gryko and D. T. Gryko, *Acc. Chem. Res.*, 2017, **50**, 2334–2345.
17 G. Sanil, B. Koszarna, Y. M. Poronik, O. Vakuliuk, B. Szymański, D. Kusy and D. T. Gryko, in *Advances in Heterocyclic Chemistry*, ed. E. F. V. Scriven and C. A. Ramsden, Academic Press, 2022, vol. 138, pp. 335–409.
18 M. Krzeszewski, Ł. Dobrzycki, A. L. Sobolewski, M. K. Cyrański and D. T. Gryko, *Angew. Chem., Int. Ed.*, 2021, **60**, 14998–15005.
19 Y. M. Poronik, G. V. Baryshnikov, I. Deperasińska, E. M. Espinoza, J. A. Clark, H. Ågren, D. T. Gryko and V. I. Vullev, *Commun. Chem.*, 2020, **3**, 190.
20 K. Skonieczny, I. Papadopoulos, D. Thiel, K. Gutkowski, P. Haines, P. M. McCosker, A. D. Laurent, P. A. Keller, T. Clark, D. Jacquemin, D. M. Guldi and D. T. Gryko, *Angew. Chem., Int. Ed.*, 2020, **59**, 16104–16113.
21 T. Oyama, L. Mendive-Tapia, V. Cowell, A. Kopp, M. Vendrell and L. Ackermann, *Chem. Sci.*, 2023, **14**, 5728–5733.
22 F. de Moliner, I. Biazruchka, K. Konsewicz, S. Benson, S. Singh, J.-S. Lee and M. Vendrell, *Front. Chem. Sci. Eng.*, 2022, **16**, 128–135.
23 P. K. Mehta, K. Ryu, C. K. Kim and K.-H. Lee, *New J. Chem.*, 2022, **46**, 7003–7013.
24 S. Benson, F. de Moliner, A. Fernandez, E. Kuru, N. L. Asiimwe, J.-S. Lee, L. Hamilton, D. Sieger, I. R. Bravo, A. M. Elliot, Y. Feng and M. Vendrell, *Nat. Commun.*, 2021, **12**, 2369.
25 (*a*) M. Tasior, O. Vakuliuk, D. Koga, B. Koszarna, K. Górski, M. Grzybowski, Ł. Kielesiński, M. Krzeszewski and D. T. Gryko, *J. Org. Chem.*, 2020, **85**, 13529–13543; (*b*) A. Janiga, E. Glodkowska-Mrowka, T. Stoklosa and D. T. Gryko, *Asian J. Org. Chem.*, 2013, **2**, 411–415.
26 W. Hagui, H. Doucet and J.-F. Soulé, *Chem*, 2019, **5**, 2006–2078.
27 G. Łukasiewicz, H. G. Ryu, A. Mikhaylov, C. Azarias, M. Banasiewicz, B. Kozankiewicz, K. H. Ahn, D. Jacquemin, A. Rebane and D. T. Gryko, *Chem. – Asian J.*, 2017, **12**, 1736–1748.

 